Chapter 6

Redox Levels and Potentials

6.0.1 ABSTRACT

So far, we have been concerned with the highly optimized photon-to-charge conversion in photosynthetic bacterial reaction centers and a biomimetic system. In plant photosystems photons are not only converted to charges, the photogenerated holes are also utilized for water oxidation. The photosystem II reaction center performs photoinduced charge separation in a similar protein-cofactor architecture as the bacterial reaction center. Yet the mechanism is less understood and the oxidation potential of the primary donor ($P680^{+}$) is the highest known to biological systems. Only recently, spectroscopic evidence for coherent charge separation processes have been discovered. In this chapter we do not discuss the dynamics of coherent charge transfer in photosystem II. Rather, we show how density functional theory can be used to model large complexes the size of reaction centers and provide a qualitatively correct picture of static redox levels, coupling between chromophores and vertical charge transfer energies. Additionally, we present evidence that the high oxidation potential of P680 implies a very small dielectric constant of the local protein environment.

Parts of this chapter are to be submitted:
T. J. Eisenmayer, J. Marcelis, H. J. M. de Groot and F. Buda, **2014**.

6.1 Introduction

Photosystem II (PSII) is the complex that powers the biosphere. Not only does it transform solar irradiation into charge separated states, it also couples this ultrafast process to the relatively slow catalytic cycle of water oxidation, whilst operating at the highest known oxidation potential in biological systems. Only recently (2011) a highly accurate crystal structure of PSII has been resolved [1]. The functioning of PSII has been studied intensively [2-6]. A remarkable difference with the bacterial reaction center (bRC), considered in the previous chapters, is its absorption spectrum [7]. Apart from the fact that the absorption maximum at 680 nm is shifted towards the blue, the PSII absorption band is broad with little fine structure, meaning that all cofactors absorb at approximately the same wavelength. This is in stark contrast with bRCs where the different cofactor pairs (P_LP_M,B_AB_B and H_AH_B) exhibit distinct absorption peaks. The electron transfer chain is therefore more easily understood ($P \rightarrow B \rightarrow H$) [8]. In PSII, there may be multiple charge separation pathways that only recently are being uncovered [9,10], and the coherent mixing of charge transfer states into the delocalized excitons due to long-living collective vibrations is recently suggested to be the cause of its high efficiency [11,12,13]. In this Chapter we will not discuss these features, but rather concentrate on the larger supramolecular architecture of the reaction centers using static density functional theory methods to assess the relative energies of frontier orbitals, to calculate charge transfer integrals between cofactor pairs and to assess the energies of the different charge transfer states. Additionally, we discuss the fact that the PSII primary donor has an oxidation potential of $\sim$ 1.2 V [14-16] enabling it to oxidize water, whereas the bRC operates at only 0.5 V [17]. For PSII, we analyze how the oxidation potential of the primary donor is affected by geometrical distortion and by varying the dielectric constant of the environment.

6.2 Models and Methods

The total photosystem II model is extracted from the latest X-ray crystallographic data (PDB-entry 3ARC [1]) and comprises the 4 chlorophyll pigments, 2 pheophytins and the 12 closest surrounding residues (653 atoms in total, see Figure 6.1 and Appendix I for the full list). For this large supramolecular complex we perform density functional theory calculations using the ADF quantum chemical suite [18] at the BLYP/TZP level of theory. The same computational setup is used for a model of bRC (PDB-entry

1M3X) comprising also all the cofactors and the direct protein environment. We also subdivide the total model into 5 smaller cofactor-pair models, including interstitial and surrounding amino acids. We shall refer to these models based on their constituent cofactors: $Pheo_{D1}Chl_{D1}$, $Chl_{D1}P_{D1}$, $P_{D1}P_{D2}$, $P_{D2}Chl_{D2}$ and $Chl_{D2}Pheo_{D2}$.

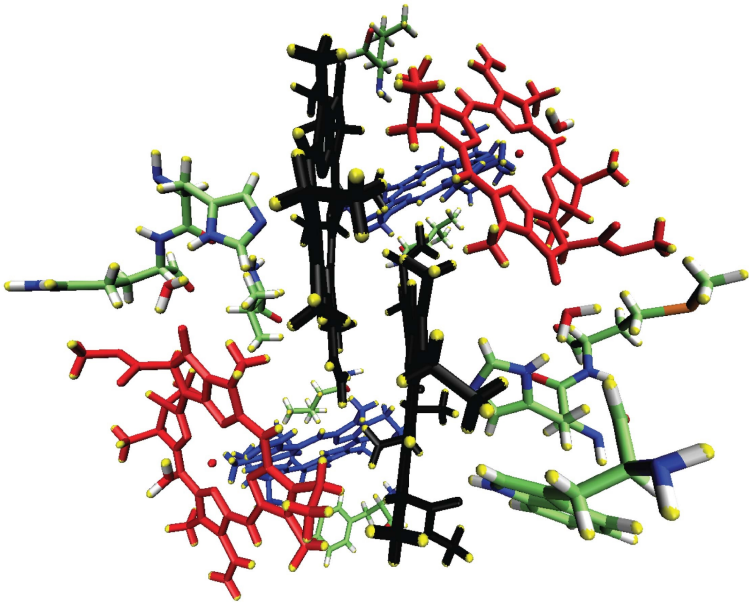

Figure 6.1: Total model of PSII including 653 atoms, 6 cofactors and 12 residues.

From these models we calculate charge transfer integrals between adjacent cofactors with the method of Senthilkumar [19,20] as implemented in ADF at the B3LYP/TZP level. Additionally, we compute the charge transfer energies of the 6 most likely charge transfer configurations in PSII, being $Pheo^{-}_{D1}Chl^{+}_{D1}$, $Chl^{-}_{D1}P^{+}_{D1}$, $P^{-}_{D1}P^{+}_{D2}$, $P^{+}_{D1}P^{-}_{D2}$, $P^{+}_{D2}Chl^{-}_{D2}$ and $Chl^{+}_{D2}Pheo^{-}_{D2}$. These energies are calculated using the method of Wu and van Voorhis [21,22] implemented in the CPMD suite [23], known as constrained DFT (CDFT). Within this formalism the DFT energy is optimized under a charge density constraint corresponding to a cofactor with charge +1 and a cofactor with -1. We use the BLYP functional [24,25] and a plane-wave basis set with an energy cutoff of 70 Ry and employ dispersion-corrected atom-centered pseudopotentials (DCACP) [26,27]. Finally, we extract only the P_{D1} chlorophyll as a model for calculating the

oxidation potential of the primary donor under different solvation conditions as expressed by a range of dielectric constants ($1 < \epsilon < 80$) within the conductor-like screening model (COSMO) [28]. The oxidation potential is calculated by subtracting the energy at the B3LYP/TZP level in the ground state closed-shell system from the energy of the cationic chlorophyll (P^+_{D1}) under the same solvation conditions. This is compared with the bacteriochlorophyll (P_L) of the *Rhodobacter Sphaeroides* reaction center and with undistorted chlorophyll after geometry optimization with ADF at the B3LYP/TZP level.

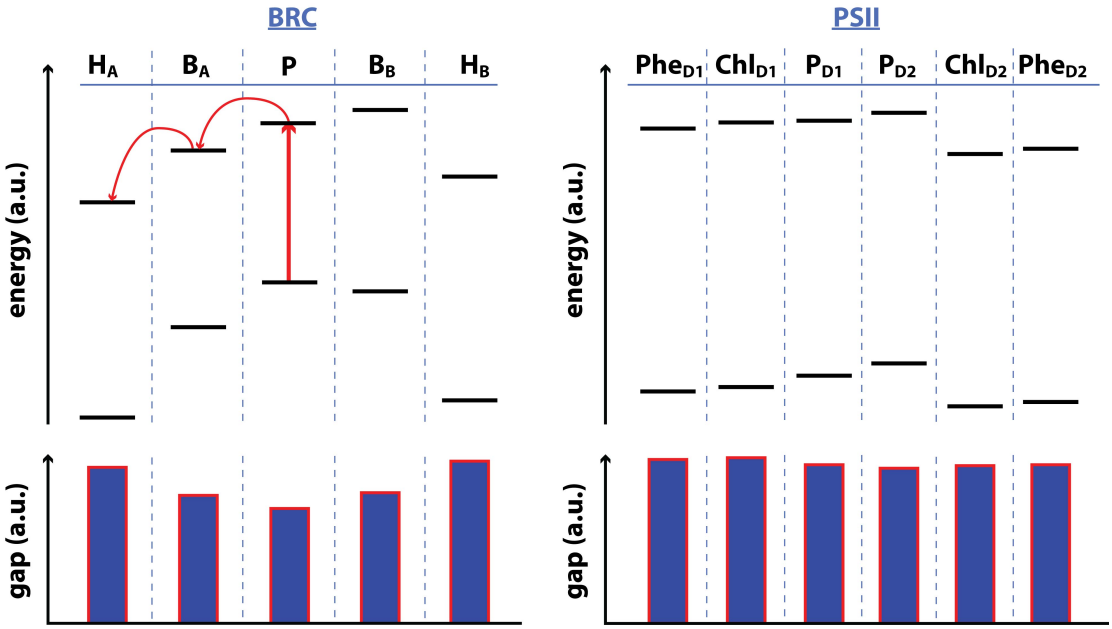

Figure 6.2: HOMO-, LUMO-levels and HOMO-LUMO gaps (vertical bars) for the full model ($\sim$ 650 atoms). In the bRC the smallest gap is at the special pair and there is a moderate redox gradient for unidirectional electron transfer (red arrows) while the LUMO on B_B is higher in energy then P. For PSII, the gaps are similar and there is a smaller gradient for unidirectional electron transfer. It is suggested that there is a lower lying LUMO on the D2 branch at Chl_{D2}.

6.3 Results and Discussion

The single-point density optimization of the total PSII model is evaluated by first considering the localization of the frontier orbitals. We find that

these orbitals are neatly localized on individual cofactors and we can thus associate orbital energies with specific cofactors. This can be done for the highest occupied (HOMO) and lowest unoccupied (LUMO) molecular orbitals. We can then define a local energy gap for every cofactor that is a crude approximation of the 'true' site energy. Notwithstanding the approximate nature of the absolute energies and energy gaps, we are interested in a qualitative description of the electronic structure of the entire complex. Figure 6.2 summarizes the energy gaps and frontier orbital energies for the cofactors in PSII (*right*) and compares these with bRC (*left*). It can be seen that the qualitative picture of the electronic structure of bRC is correct. The special pair (P) gap is smallest, the gaps of the two accessory bacteriochlorophylls (B) on either side are expectedly larger and of the same magnitude and the gaps of the bacteriopheophytins (H) are even larger and also of the same magnitude. This corresponds to the absorption spectrum of bRC [29], where the special pair peak is the most red-shifted, followed by a peak consisting of $B_{A,B}$ and farthest to the blue a peak corresponding to $H_{A,B}$. Therefore, by using the generalized gradient approximation (GGA, i.e. BLYP) for the exchange-correlation energy within DFT one can qualitatively describe the electronic structure of a protein-cofactor complex the size of the bRC (red arrows, Figure 6.2)and make an educated guess about the directionality of the charge separation in the complex along the B-branch [8,29]. If we consider the PSII orbital energies (Figure 6.2, right) and HOMO-LUMO gaps the picture is different, yet qualitatively consistent with the PSII experimental absorption spectrum showing only one broad peak that contains all cofactors [7].

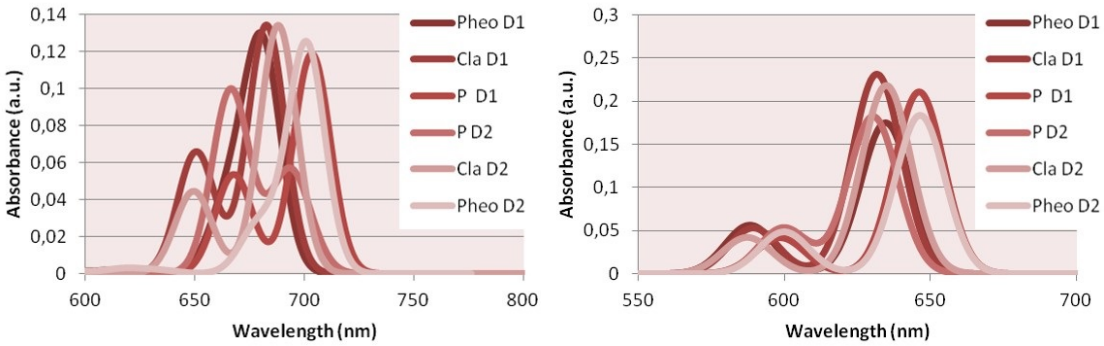

Figure 6.3: TDDFT spectra (*left*: BLYP/TZP, *right*: B3LYP/TZP).

With linear response TDDFT calculations on the 6 cofactor models (with local protein environment included) we are able to reproduce this as shown in Figure 6.3. Interestingly, the BLYP functional provides more accurate site energies centered around 680 nm compared to the hybrid B3LYP functional that overestimates the excitation energies. The narrow range of site-energies in PSII is therefore reproduced and Figure 6.3 clearly illustrates the difference with the electronic structure of bRC. What both reaction centers do have in common is the unidirectionality of electron transfer, despite the twofold-symmetric architectures. Within the orbital energies pictures discussed above a higher LUMO-energy at B_B is observed for bRC and a lower LUMO-energy at Chl_{D2} for PSII. In this static picture these discontinuities in the redox gradients along the inactive branches may be related to the directionality of electron transfer steps. However, dynamic effects would need to be taken into account to substantiate this.

While the orbital energy picture gives some insight into the possible electron transfer paths, also the electron coupling between different cofactors will be considered for the static structure. In Figure 6.4, we show the charge transfer integrals between adjacent cofactor pairs that are a measure for the electronic coupling.

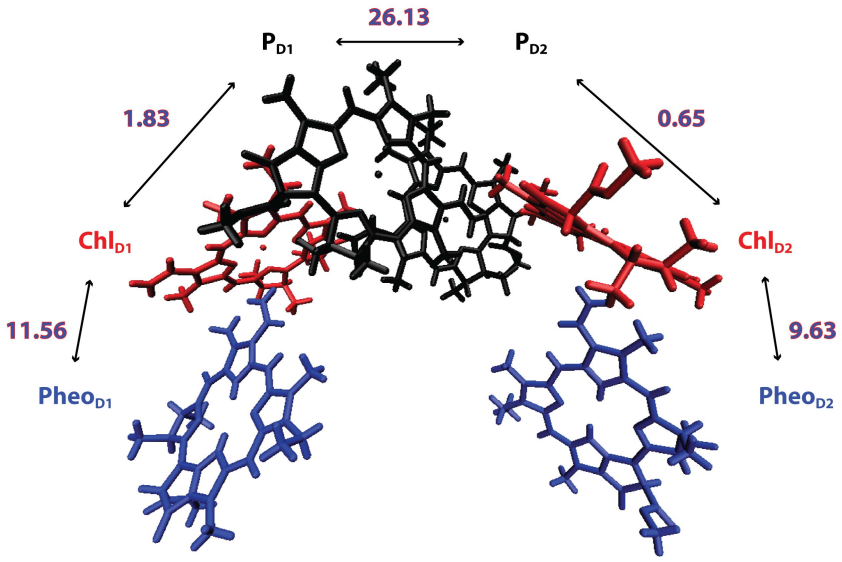

Figure 6.4: Charge transfer integrals between the cofactor LUMO's (meV).

The magnitude of the charge transfer integrals compares nicely with the related heme-heme macrocycle electronic coupling found to be $\sim$ 10 meV [30]. Our calculations show a strong coupling between the chlorophylls constituting the special pair and weaker couplings with the accessory chlorophylls and pheophytins. By comparing the D1 and D2-branches it can be seen that the coupling strength between the special pair and the accessory Chl_{D2} is significantly lower than with its counterpart on the D1-branch. The center-to-center distances between the special pair chlorophylls and the accessory chlorophylls may contribute to this effect as the $P_{D1} - Chl_{D1}$ distance (10.38 Å) is 0.13 Å shorter than the $P_{D2} - Chl_{D2}$ distance (10.51 Å) according to the latest crystal structure [1]. Another factor of influence may be that the water ($Water_{D1}$) that coordinates to Chl_{D1} is hydrogen bonded to a tryptophan ($Thr179_{D1}$), whereas the water that coordinates to Chl_{D2} has no surrounding residues in its proximity that it can form a hydrogen bond with [1].

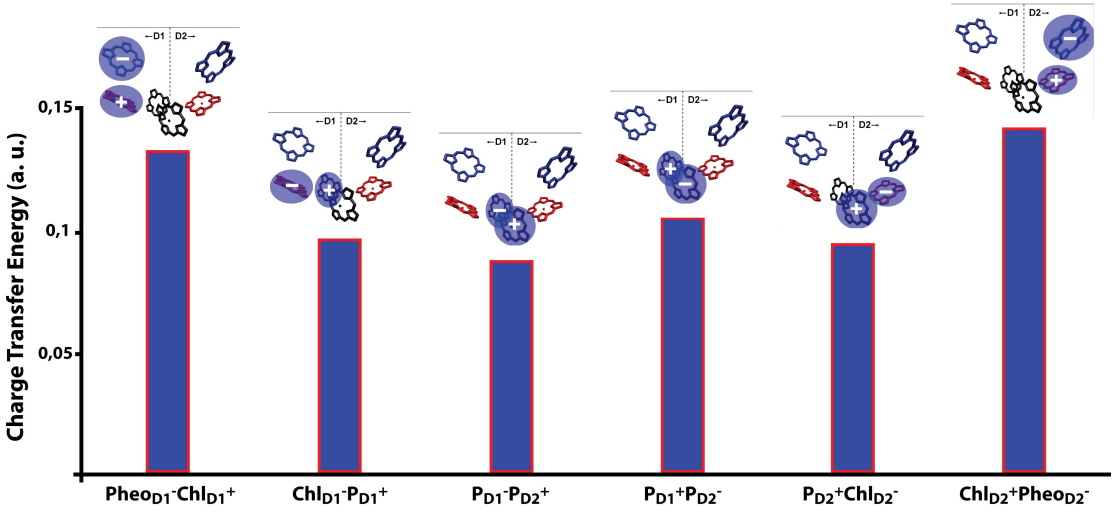

Figure 6.5: Vertical charge transfer energies from constrained DFT of nearest-neighbour cofactor pairs in atomic units, calculated including the direct protein environment. The internal charge transfer state in the special pair with the electron on P_{D1} and the hole on P_{D2} is found to be the lowest in energy.

Where the charge separation in PSII is initiated has been much debated as all site energies are very similar. The charge transfer energies in Figure 6.5 are calculated by constraining a positive charge on one cofactor and a

negative charge on its nearest neighbour. In agreement with the minimum HOMO-LUMO gap for P_{D2} that can be discerned from Figure 6.2, the lowest accessible charge transfer state is found to be internal to the special pair and has a hole on P_{D2} and an electron on P_{D1} ($P_{D1}^{+}P_{D2}^{-}$). A proper comparison with the dominant charge separation mechanisms found in ultrafast spectroscopic experiments [9,10,11] would however require dynamic effects, as energy levels are so closely spaced.

How charge transfer states mix into excitonic states in PSII to produce stable charge separated states with high yield is an area of current debate, and likely involves a coherent coupling to vibrational modes [12,13] as we have seen in the bRC. First-principles molecular dynamics simulations as described in the previous chapters and in the following chapter could contribute to a better mechanistic understanding of this process.

6.3.1 Oxidation Potential

The location of the cation, P_{D1}^{+}, formed after charge separation is well established [3,31]. We extract the P_{D1} chlorophyll from the latest crystal structure (PDB-entry: 3ARC) and calculate the energy difference between the ground state closed-shell system and the cationic state P_{D1}^{+} in vacuum. We repeat this calculation adding a continuous solvent with increasing dielectric constant, resulting in the blue curves in Figure 6.6. In the upper panel we compare PSII with the P_{L}^{+} bacteriochlorophyll of bRC. There is an intrinsic difference in oxidation potential between chlorophyll and bacteriochlorophyll of 0.16 eV [16] that is well reproduced. Interestingly, the oxidation potential of $P680^{+}$ (PSII) is experimentally found at $\sim$ 1.2 V [14-16], which is a lot larger than $P870^{+}$ (bRC) at $\sim$ 0.5 V [17] even when the intrinsic difference in potential between bacteriochlorophyll and chlorophyll is taken into account. Taking the curves in the upper panel of Figure 6.6 and relating them to these experimental values implies a very low dielectric constant of $\epsilon \sim 2$ for the local environment of P_{D1} in PSII and a relatively high dielectric constant of $\epsilon \sim 10$ for P_{L} in bRC. We conclude that the ability of PSII to oxidize water is related to the low dielectric constant of the protein environment surrounding the primary donor in agreement with an earlier DFT-study [32]. This is further substantiated by considering the lower panel in Figure 6.6, where we plot the dependence on the dielectric constant of optimized chlorophyll (light blue line), which does not differ significantly from the results obtained from the distorted chlorophyll extracted from the crystal structure (dark blue line). This suggests that the high oxi-

dation potential is not so much due to geometric distortions induced by the protein scaffolding. Rather, electrostatic effects are found to be important.

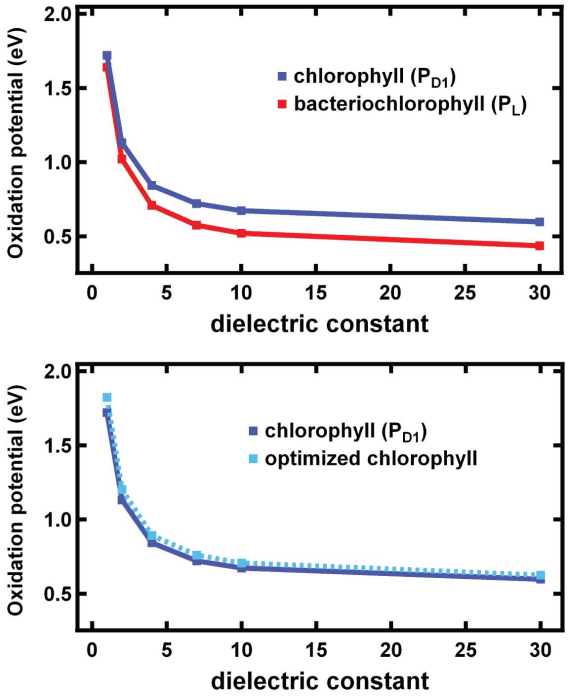

Figure 6.6: Oxidation potential estimated by subtracting the total DFT-energy of the closed-shell system from the oxidized system at the B3LYP/TZP level of theory in a continuous solvent model (COSMO) with varying dielectric constant. The PSII chlorophyll P_{D1} (dark blue line) as extracted from the latest crystal structure (PDB-entry: 3ARC) is compared with the bRC bacteriochlorophyll P_L (red line, PDB-entry 1M3X) and with optimized chlorophyll (light blue line).

6.4 Conclusions

We have used various DFT-based methods to assess site energies, electronic couplings, charge transfer energies and oxidation potentials in PSII and have compared some of these results with the bRC. Overall we find a good agreement with experiment and an insightful qualitative picture of the PSII reaction center. The origin of the high oxidation potential of the PSII primary donor $P680^+$ is suggested to be the low local dielectric constant ($\epsilon \sim 2$) of the protein matrix.

6.5 References

[1] Umena, Y., Kawakami, K., Shen, J.-R., and Kamiya, N., Crystal structure of oxygen-evolving photosystem II at a resolution of 1.9 Å, *Nature* **2011**, 473, 55-60.

[2] Durrant, J.R., Klug, D.R., Kwa, S.L., Van Grondelle, R., Porter, G., and Dekker, J.P. A multimer model for P680, the primary electron donor of photosystem II, *PNAS* **1995**, 92, 4798-4802.

[3] Groot, M.L., Pawlowicz, N.P., van Wilderen, L.J., Breton, J., van Stokkum, I.H., and van Grondelle, R., Initial electron donor and acceptor in isolated photosystem II reaction centers identified with femtosecond mid-IR spectroscopy, *PNAS* **2005**, 102, 13087-13092.

[4] Holzwarth, A.R., Muller, M.G., Reus, M., Nowaczyk, M., Sander, J., and Rogner, M., Kinetics and mechanism of electron transfer in intact photosystem II and in the isolated reaction center: pheophytin is the primary electron acceptor. *PNAS* **2006**, 103, 6895-6900.

[5] Diller, A., Roy, E., Gast, P., van Gorkom, H.J., de Groot, H.J., Glaubitz, C., Jeschke, G., Matysik, J., and Alia, A., 15N photochemically induced dynamic nuclear polarization magic-angle spinning NMR analysis of the electron donor of photosystem II, *PNAS* **2007**, 104, 12767-12771.

[6] Renger, T., and Schlodder, E., Primary Photophysical Processes in Photosystem II: Bridging the Gap between Crystal Structure and Optical Spectra. *ChemPhysChem* **2010**, 11, 1141-1153.

[7] Konermann, L., and Holzwarth, A.R., Analysis of the absorption spectrum of photosystem II reaction centers: Temperature dependence, pigment assignment, and inhomogeneous broadening, *Biochemistry* **1996**, 35, 829-842.

[8] Holzapfel, W., Finkele, U., Kaiser, W., Oesterhelt, D., Scheer, H., Stilz, H.U., and Zinth, W., Initial electron-transfer in the reaction center from Rhodobacter sphaeroides, *PNAS* **1990**, 87, 5168-5172.

[9] Romero, E., van Stokkum, I.H.M., Novoderezhkin, V.I., Dekker, J.P., and van Grondelle, R, Two Different Charge Separation Pathways in Photosystem II, *Biochemistry* **2010**, 49, 4300-4307.

[10] Novoderezhkin, V.I., Romero, E., Dekker, J.P., and van Grondelle, R., Multiple Charge-Separation Pathways in Photosystem II: Modeling of Transient Absorption Kinetics, *ChemPhysChem* **2011**, 12, 681-688.

[11] Novoderezhkin, V.I., Dekker, J.P., and van Grondelle, R., Mixing of Exciton and Charge-Transfer States in Photosystem II Reaction Centers: Modeling of Stark Spectra with Modified Redfield Theory, *Biophysical Journal* **2007**, 93, 1293-1311.

[12] Romero, E., Augulis, R., Novoderezhkin, V.I., Ferretti, M., Thieme, J., Zigmantas, D., and van Grondelle, R., Quantum coherence in photosynthesis for

efficient solar-energy conversion, *Nature Physics* **2014**, *advanced publication*.

[13] Fuller, F.D., Pan, J., Gelzinis, A., Butkus, V., Senlik, S.S., Wilcox, D.E., Yocum, C.F., Valkunas, L., Abramavicius, D., and Ogilvie, J.P., Vibronic coherence in oxygenic photosynthesis, *Nature Chemistry* **2014**, 6, 706-711.

[14] Rappaport, F., Guergova-Kuras, M., Nixon, P.J., Diner, B.A., and Lavergne, J., Kinetics and Pathways of Charge Recombination in Photosystem II, *Biochemistry* **2002**, 41, 8518-8527.

[15] Ishikita, H., Loll, B., Biesiadka, J., Saenger, W., and Knapp, E. W., Redox Potentials of Chlorophylls in the Photosystem II Reaction Center, *Biochemistry* **2005**, 44, 4118-4124.

[16] Ishikita, H., Saenger, W., Biesiadka, J., Loll, B., and Knapp, E. W., How photosynthetic reaction centers control oxidation power in chlorophyll pairs P680, P700, and P870, *PNAS* **2006**, 103, 9855-9860.

[17] X. Lin, H. A. Murchison, V. Nagarajan, W. W. Parson, J. P. Allen, and J. C. Williams, Specific alteration of the oxidation potential of the electron donor in reaction centers from *Rhodobacter sphaeroides*, *PNAS* **1994**, 91(22), 10265-10269.

[18] ADF2012, SCM, Theoretical Chemistry, Vrije Universiteit, Amsterdam, The Netherlands, http://www.scm.com/.

[19] K. Senthilkumar, F.C. Grozema, F.M. Bickelhaupt, and L.D.A. Siebbeles, Charge transport in columnar stacked triphenylenes: Effects of conformational fluctuations on charge transfer integrals and site energies, *The Journal of Chemical Physics* **2003**, 119, 9809.

[20] K. Senthilkumar, F.C. Grozema, C. Fonseca Guerra, F.M. Bickelhaupt, F.D. Lewis, Y.A. Berlin, M.A. Ratner, and L.D.A. Siebbeles, Absolute Rates of Hole Transfer in DNA, *JACS* **2005**, 127, 14894.

[21] Wu, Q.; Van Voorhis, T. Constrained Density Functional Theory and its Application in Long-Range Electron Transfer. *J. Chem. Theory Comput.* **2006**, 2, 765-774.

[22] Wu, Q.; Van Voorhis, T. Direct Optimization Method to Study Constrained Systems Within Density-functional Theory. *Phys. Rev. A* **2005**, 72, 024502.

[23] CPMD v3.11.1, Copyright IBM Corp, 1990-2008; Copyright MPI für Festkörperforschung Stuttgart, 1997-2001. http://www.cpmd.org/.

[24] Becke, A. D. Density-Functional Exchange-Energy Approximation with Correct Asymptotic Behavior. *Phys. Rev. A* **1988**, 38, 3096.

[25] Lee, C.; Yang, W.; Parr, R. G. Development of the Colle-Salvetti Correlation-energy Formula into a Functional of the Electron Density. *Phys. Rev. B* **1988**, 37, 785.

[26] von Lilienfeld, O. A.; Tavernelli, I.; Rothlisberger, U.; Sebastiani, D. Optimization of Effective Atom Centered Potentials for London Dispersion Forces in Density Functional Theory. *Phys. Rev. Lett.* **2004**, 93, 153004.

[27] von Lilienfeld, O. A.; Tavernelli, I.; Rothlisberger, U.; Sebastiani, D. Performance of Optimized Atom-centered Potentials for Weakly Bonded Systems Using Density Functional Theory. *Phys. Rev. B* **2005**, 71, 195119.

[28] C.C. Pye and T. Ziegler, An implementation of the conductor-like screening model of solvation within the Amsterdam density functional package, *Theoretical Chemistry Accounts* **1999**, 101, 396.

[29] M. A. Steffen, K. Lao, and S. G. Boxer, Dielectric Asymmetry in the Photosynthetic Reaction Center, *Science* **1994**, 264 (5160), 810-816.

[30] Smith, D. M. A.; Rosso, K. M.; Dupuis, M.; Valiev, M.; Straatsma, T. P., Electronic Coupling between Heme Electron-Transfer Centers and Its Decay with Distance Depends Strongly on Relative Orientation, *J. Phys. Chem. B* **2006**, 110, 15582-15588.

[31] Saito, K., Ishida, T., Sugiura, M., Kawakami, K., Umena, Y., Kamiya, N., Shen, J.-R., and Ishikita, H., Distribution of the Cationic State over the Chlorophyll Pair of the Photosystem II Reaction Center, *JACS* **2011**, 133, 14379-14388.

[32] Hasegawa, K., and Noguchi, T., Density Functional Theory Calculations on the Dielectric Constant Dependence of the Oxidation Potential of Chlorophyll: Implication for the High Potential of P680 in Photosystem II, *Biochemistry* **2005**, 44, 8865-8872.

6.6 Appendix I

List of residues comprising the total PSII model:

Cofactors:

P_{D1} (CLA 604), P_{D2} (CLA 605), Chl_{D1} (CLA 606), Chl_{D2} (CLA 607), $Pheo_{D1}$ (PHO 608), $Pheo_{D2}$ (PHO 609).

Amino acids coordinated to cofactors:

His_{D1} coordinated to P_{D1} (HIS 198), His_{D2} coordinated to P_{D2} (HIS 197), $Water_{D1}$ coordinated to Chl_{D1} (HOH 1003), $Water_{D2}$ coordinated to Chl_{D2} (HOH 1009), Leu_{D1} coordinated to $Pheo_{D1}$ (LEU 209), Leu_{D1} coordinated to $Pheo_{D1}$ (LEU 210).

Other residues:

LEU 151, PHE 146, MET 198, HOH 382, TRP 191, HOH 349, GLN 199, VAL 202.